First Experimental Results on Long-object Imaging using a Reverse Helical Trajectory with a C-arm System

Zhicong Yu, Andreas Maier, Manfred Schönborn, Florian Vogt, Christoph Köhler, Günter Lauritsch, Joachim Hornegger, and Frédéric Noo

***Abstract*—3D imaging with C-arm systems has become a crucial tool in the interventional room. In this work, we present a methodology and first experimental results for long-object imaging using a reverse helical trajectory with a modified Artis zeego system. First the raw data was preprocessed by the Siemens pipeline, and the scan positions were obtained through a calibration process. After trajectory registration and fitting, preprocessed data was rebinned, and image reconstructions were obtained through the Fusion-RFDK method. The reconstruction results are encouraging and effectively demonstrate that long-object imaging using a reverse helical trajectory is feasible in the interventional room.**

I. Introduction

3D imaging with C-arm systems has become a crucial tool in the interventional room. It has allowed significant improvements in clinical workflow, and it has also enabled new interventional procedures as well as refinements in existing procedures. In this work, we seek to further improve the capabilities of this 3D imaging tool by allowing smooth, long-object scanning using a reverse helix [1] for data acquisition. The reverse helix is well-suited for C-arm systems, particularly since such systems are open and do not include slip-ring technology.

This work presents a methodology and first experimental results for long-object imaging using a reverse helical trajectory with multi-turns using a modified Artis zeego system (Siemens AG, Healthcare Sector, Forchheim, Germany). The methodology involved the following five steps: i) a calibration method [2] to assess the exact geometrical position of the source and the detector during data acquisition, ii) the computation of a rigid transformation to register these positions into a conventional reverse helix geometry, iii) a geometrical fitting process to find an analytical reverse helix to match the registered trajectory, iv) a rebinning step to interpolate the measured data into the fitted geometry, and v) an application of the Fusion-RFDK [3] method for reconstruction from the rebinned data. Using this methodology, we were able to produce satisfactory reconstructions of two physical objects that extend over a 300 mm long volume. These reconstructions were obtained from real data collected over five turns.

Zhicong Yu and Frederic Noo are with Department of Radiology, University of Utah, Salt Lake City, UT, USA; Andreas Maier, Manfred Schönborn, Florian Vogt, Christoph Köhler and Günter Lauritsch are with Siemens AG, Healthcare Sector, Forchheim, Germany; Zhicong Yu and Joachim Hornegger are with The Chair of Pattern Recognition, University of Erlangen-Nuremberg, Erlangen, Germany. This work was partially supported by a grant of Siemens AG, Healthcare Sector and by the U.S. National Institutes of Health (NIH) under grant R21 EB009168. The concepts presented in this paper are based on research and are not commercially available. Its contents are solely the responsibility of the authors and do not necessarily represent the official views of the NIH.

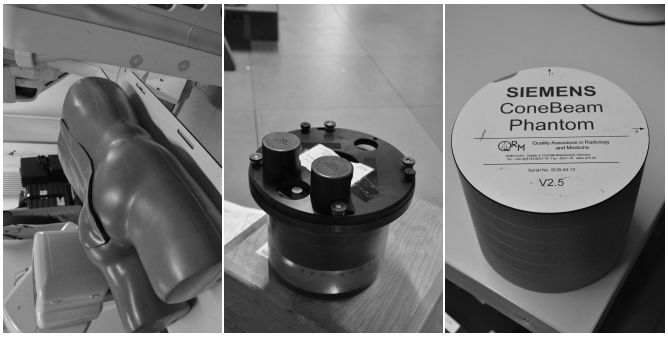

Fig. 1. Left: TORSO with SAWBONES spine. Middle: CATPHAN phantom. Right: Siemens Cone-Beam phantom. The CATPHAN and Siemens CB phantoms were scanned in-line to simulate a single long object.

II. Data acquisition

A. System configuration and data correction

As a prototype, the reverse helical trajectory was successfully implemented on the modified Artis zeego system by rotating and translating the C-arm gantry around a stationary patient table. We avoided any table motion because patients are usually connected to several medical instruments so that translating them poses health risks. The trajectory achieved in this experiment consists of five turns, and each turn was configured with the same angular coverage (240° of step-size 0.35°) and the same axial height (60 mm). This configuration yielded 681 projections per turn, with each projection acquired on a 300×400 mm^2 flat-panel detector of binned pixel size $0.308\,\text{mm} \times 0.308$ mm. The detector was set in the landscape mode (shorter side in the axial direction) so as to maximize the radius of the field-of-view (FOV) (about 130 mm) in the trans-axial direction. The rotation radius was about 785 mm, and the source-to-detector distance was about 1199 mm.

Three phantoms were scanned: the anthropomorphic torso phantom containing a SAWBONES spine [4], the CATPHAN phantom [5] and the Siemens Cone-Beam (CB) phantom [6] (QRM, Möhrendorf, Germany), as shown in Figure 1. The torso phantom is of length 550 mm, width 400 mm and

thickness 200 mm, and the inserted spine is of length 360 mm and of diameter 180 mm. This phantom was placed parallel to the patient table so that the entire spine was located within the FOV. Due to the large transversal size, the torso phantom suffered from trans-axial data truncation, which was not the case for the CATPHAN and Siemens CB phantoms, since they had small enough radii to be wholly contained within the FOV. On the other side, the CATPHAN and Siemens CB phantoms are too short to test long-object imaging, and thus they were scanned in-line so as to define a long object.

Preprocessed projection data was obtained by converting the photon number to line integrals using the Siemens pipeline, the major steps of which included I_0 correction for the automatic exposure control (an analog is reported in [7]), beam-hardening and scatter correction as described in [8], [9]. As an example, several preprocessed projections of the torso phantom are shown in Figure 2.

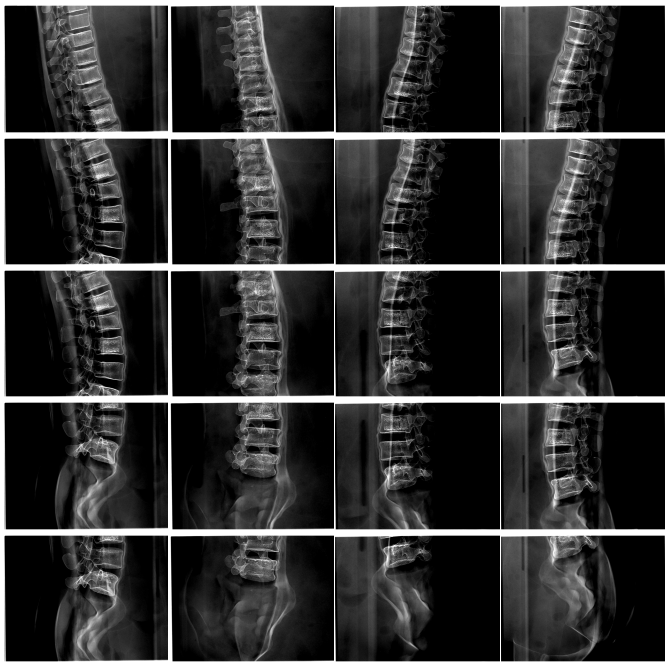

Fig. 2. Illustration of the preprocessed projections of the torso phantom. Top to bottom: 1st to 5th turn. Polar angle from left to right: $0°$, $-80°$, $-160°$ and $-230°$.

B. Trajectory calibration

Due to the open design, a C-arm system is not capable of producing a perfect source trajectory. To assess the exact geometrical positions and detector orientations, a calibration process is necessary. We have solved this calibration problem by using the robust technique presented in [2] with a new calibration phantom that was specifically designed to accommodate our long-object imaging needs. This new phantom was designed as an extension of the 206 mm long PDS-2 phantom (see [10] for an illustration), which consists of 108 beads of various size arranged on a helix with an 8-bit encoding scheme, so that identification of beads in the projection data is straightforward. The extended PDS-2 phantom is 500 mm and uses beads arranged with a 10-bit encoding scheme; see Figure 3 (upper left). The calibration process provided the source positions as well as the detector orientations in a calibration coordinate system, denoted as (xc, yc, zc), which was attached to the extended PDS-2 phantom. The calibrated trajectory is shown in Figure 3. Note that the reverse helix moves downwards opposite to the zc-axis.

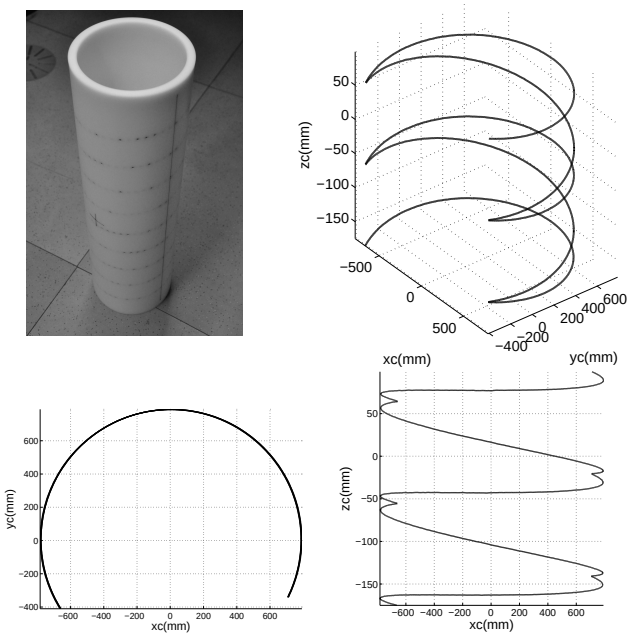

Fig. 3. Upper left: the 500 mm Siemens 10 digits PDS-2 calibration phantom. Upper right: calibrated source trajectory in the same Cartesian coordinate system as that of the calibration phantom. Lower left: projection of the calibrated trajectory onto the (xc, yc)-plane. Lower right: projection of the calibrated trajectory onto the (xc, zc)-plane.

C. Trajectory registration

In practice, it is impossible for the axial direction of the reverse helix to be parallel to the zc-axis of the calibration coordinate system, since the latter is specified by a simple manual placement of the calibration phantom on the patient table. To make the projection data appropriate for the Fusion-RFDK method, the reverse helix was first registered. This registration process transformed the trajectory from the calibration coordinate system to a Cartesian coordinate system that was defined with the (x, y, z)-axes such that i) the axial direction of the reverse helix lies on the z-axis, i.e., the projections of the vertex points onto the (x, y)-plane form a curve that is close to a circular arc, ii) the first source position lies in the (x, z)-plane.

The registered trajectory is shown in Figure 4; note in the right figure that, instead of the configured uniform axial height of 60 mm for each helical turn, the axial height of the 1st, 3rd and 5th turns is around 66 mm and that of the 2nd and 4th is about 53 mm. Various reasons could be responsible for this inconsistency, and they will be analyzed in the future. The registered trajectory is very close to a conventional reverse helix, as demonstrated in Figure 5 where the rotation radius,

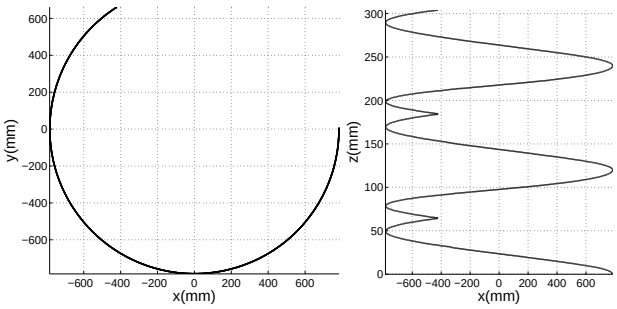

Fig. 4. Illustration of the registered trajectory. Left: projection of the registered trajectory onto the (x, y)-plane. Right: projection of the registered trajectory onto the (x, z)-plane.

the source-to-detector distance, the rotation angle and the z coordinate of each source position are displayed. Observe that the noise of both the scan radius and source-to-detector distance contains two components, i.e., white noise and low frequency noise, and we believe the former comes from the calibration process, whereas the latter stems from the effect of the gravity.

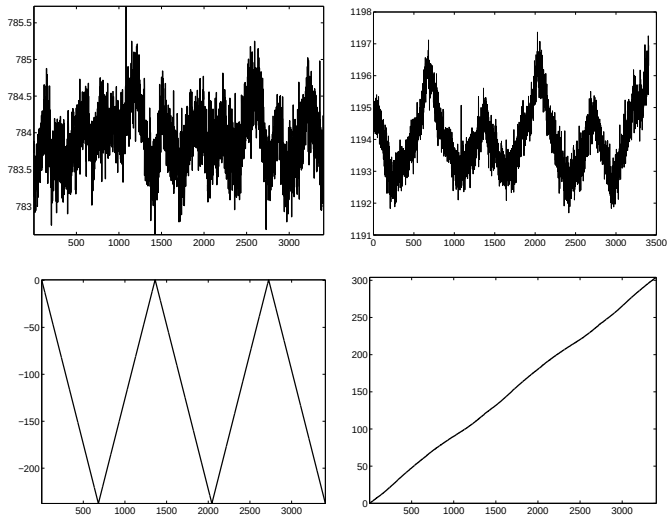

Fig. 5. Illustration of the parameters of the registered trajectory. The horizontal axis indicates the index of the source positions along the reverse helix. Upper left: rotation radius (mm); upper right: source-to-detector distance (mm); lower left: rotation angle (degree); lower right: z position (mm).

III. Image reconstruction theory

To create projection data that is suitable for reconstruction with the Fusion-RFDK method, we determined an analytically defined trajectory that fitted the registered trajectory as well as possible, and created projection data for each source position along the fitted trajectory through a rebinning process using data from the registered trajectory.

A. Trajectory fitting

Fusion-RFDK performs reconstructions independently for each helical turn, and the global results are then obtained by a fusion process. Therefore, the trajectory fitting was

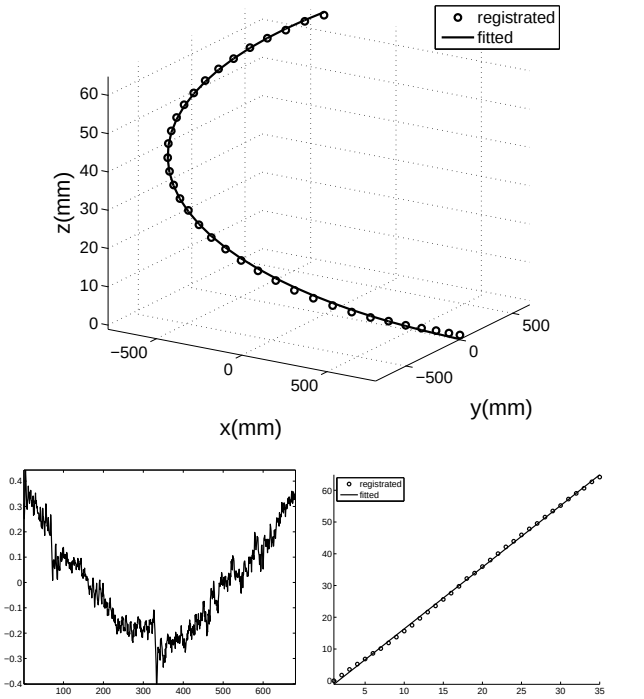

Fig. 6. Illustration of the curve fitting for the first sweep of the reverse helix. Upper: 3D view; lower left: relative angular difference for each pair of source points from the fitted and registered trajectories; lower right: illustration of z positions of both registered and fitted trajectories (mm).

achieved by respectively finding an optimal analytical helix for each turn with constant step sizes in rotation angles and z positions. The fitting was such that the total distance between each pair of source points of the fitted and registered helices was minimized. The fitted result for the first helical turn is shown in Figure 6. The top and bottom right figures indicate good agreements between the fitted and registered trajectories. However, the relative angular difference between the fitted and registered trajectories was considerable.

B. Rebinning

To create projection data for the fitted trajectory, a rebinning approach was employed for each source position. Let $\mathcal{L}(\lambda_k, \underline{\alpha}_k)$, with λ_k as the rotation angle, be the divergent beam pointing from the source point $\underline{a}(\lambda_k)$ on the fitted reverse helix in the direction $\underline{\alpha}_k$; and let $\underline{m}$ be the middle point of the two intersections between $\mathcal{L}(\lambda_k, \underline{\alpha}_k)$ and the central FOV cylinder surface, as shown in Figure 7. Also, let $\underline{b}(\gamma_i)$ and $\underline{b}(\gamma_j)$, with angular positions γ_i and γ_j, be the two points on the registered trajectory that were closest to $\underline{a}(\lambda_k)$. Then the line integral along $\mathcal{L}(\lambda_k, \underline{\alpha}_k)$ can be obtained through a linear interpolation (respect to the rotation angle) between the line integrals along the lines connecting $\underline{b}(\gamma_i)$ and $\underline{m}$, and $\underline{b}(\gamma_j)$ and $\underline{m}$. One rebinned slice is shown in Figure 8, note that the different orientation of the spine in the rebinned slice is due to different detector coordinate systems being used for the registered and fitted trajectories.

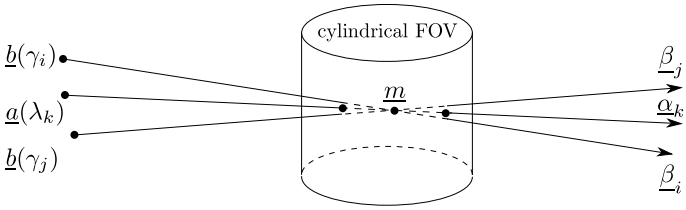

Fig. 7. Projection rebinning scheme. Source point $\underline{a}(\lambda_k)$ belongs to the fitted trajectory, and $\underline{b}(\gamma_i)$ and $\underline{b}(\gamma_j)$ are two points on the registered trajectory.

Fig. 8. The 50th rebinned projection of the torso phantom from the first sweep. Left: preprocessed; right: rebinned.

C. Reconstruction

A Fusion-RFDK reconstruction consists of four steps: i) CB length correction and Parker like weighting; ii) horizontal ramp filtering; iii) backprojection; iv) fusion. For more details, see Section III-A in [3]. Based upon those four steps, five volumes were reconstructed using the rebinned data from each turn of the fitted reverse helix separately, then all those volumes were combined by a fusion process.

In practice, two aspects need to be specified. First, we have to define kink planes, which are through the connecting point of any two successive helical turns and perpendicular to the axial axis of the reverse helix. In this work, take the kink plane of the 2nd and 3rd helices as an example, the z location of the kink plane for this portion of the reverse helix was chosen to be the average of the z positions of the last point of the 2nd turn and the first point of the 3rd turn. Other kink planes were defined in a similar way. Second, the fusion length needs to be defined. Given the radius of the FOV, $r = 130\,\text{mm}$, the height of the detector (in z), $300\,\text{mm}$, and the maximum height of all fitted sweeps, $66\,\text{mm}$, a fusion length of $30\,\text{mm}$ was chosen.

IV. Reconstruction results

Reconstructions were obtained for both the torso and the combined CATPHAN and Siemens CB phantoms with a hamming window in ramp filtering and a fusion length of 30 mm. The accuracy of the results was verified using CT images. The reconstruction of the torso phantom consists of $200 \times 200 \times 1021$ voxels of size $0.7910\ \text{mm} \times 0.7910\ \text{mm} \times 0.3\ \text{mm}$ as shown in Figure 9. For the CATPHAN and Siemens CB combined phantom, we performed two reconstructions of different voxel sizes. The reconstruction for the CATPHAN is composed of $478 \times 478 \times 1021$ voxels of size $0.3770\ \text{mm} \times 0.3770\ \text{mm} \times 0.3\ \text{mm}$ (see Figure 10 (a) and (b)), whereas the reconstruction for the Siemens CB phantom consists of $512 \times 512 \times 1021$ voxels of size

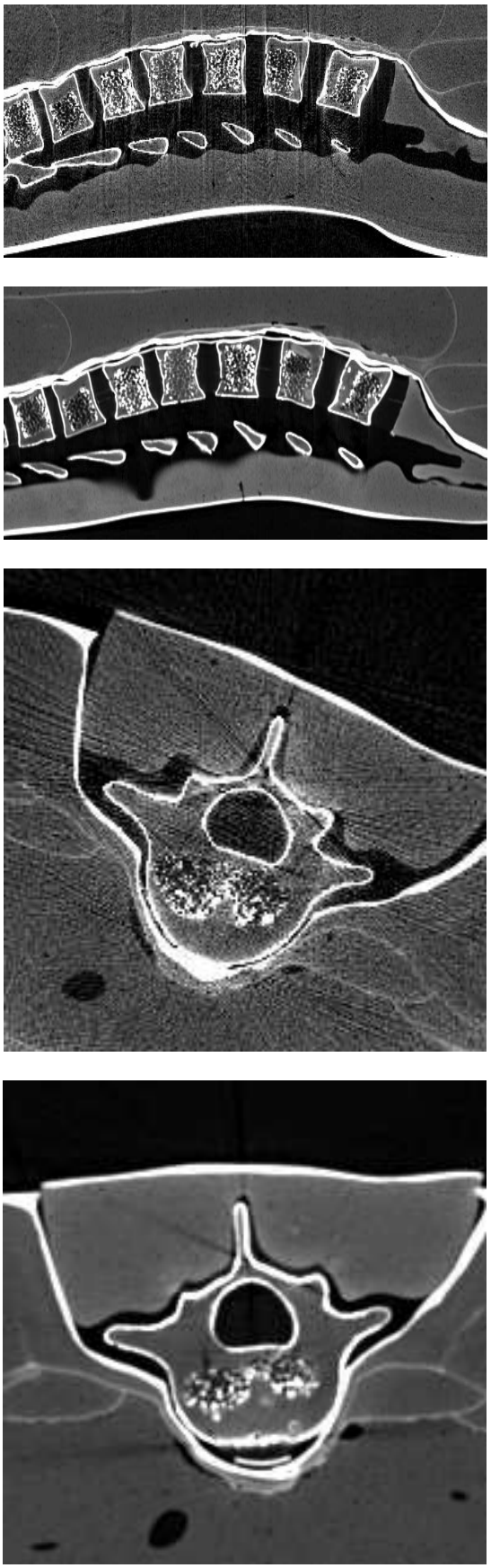

Fig. 9. Reconstruction results of the torso phantom. Display window: $(-1000, -200)$ HU. The first and second rows: sagittal view of the results from Fusion-RFDK and CT, respectively. The third and fourth rows: transversal view of the results from Fusion-RFDK and CT.

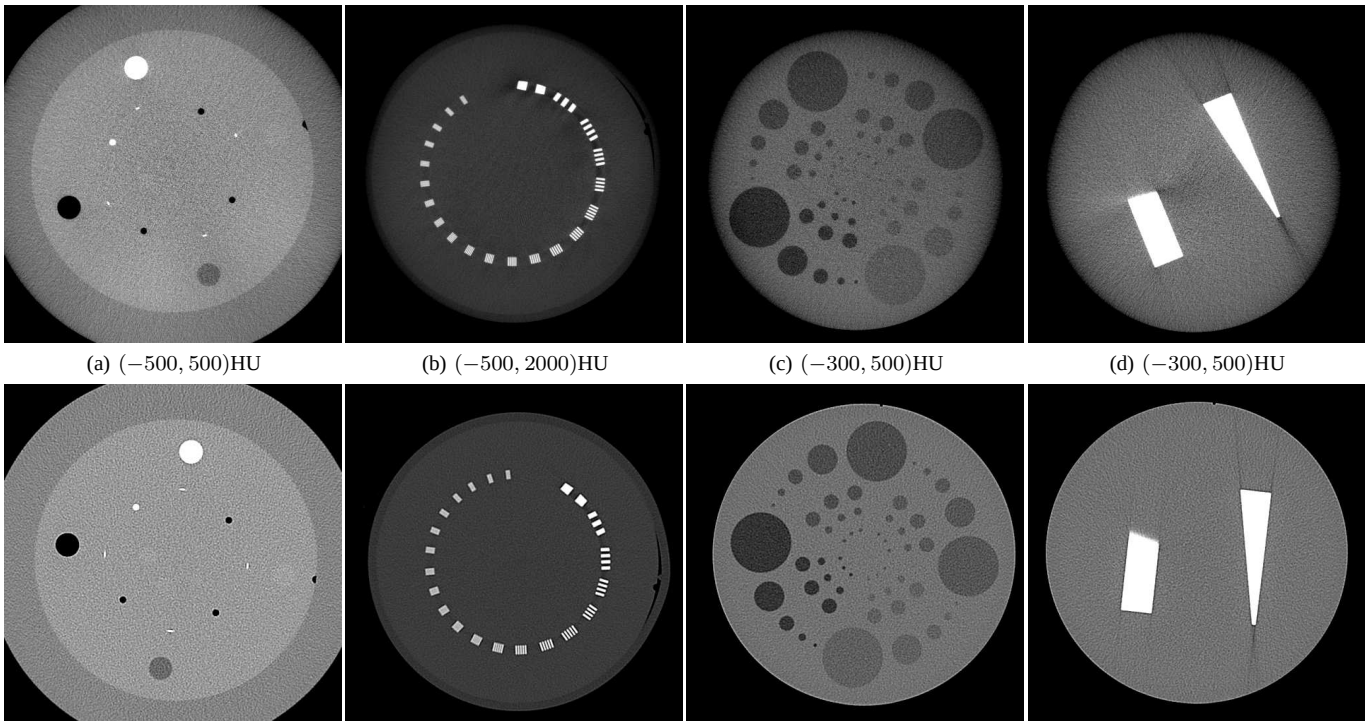

(a) $(-500, 500)$HU (b) $(-500, 2000)$HU (c) $(-300, 500)$HU (d) $(-300, 500)$HU

Fig. 10. Reconstruction results of the CATPHAN (a, b) and Siemens CB phantoms (c, d). Upper row: C-arm; lower row: CT.

0.3477 mm$\times 0.3477$ mm$\times 0.3$ mm (see Figure 10 (c) and (d)). Note that the voxel sizes used for Fusion-RFDK were matched with that of the CT images, and the attenuation coefficients were brought to the same level for both modalities using a linear mapping. It is also necessary to point out that the x-ray beam energy for the C-arm scans was 85kVp, whereas the energy for the CT scans was 120kVp.

Figures 9 and 10 indicate good agreement between our reconstuction results and the CT images. Be aware that the images from the two modalities are not registered to the same coordinate system. As preliminary results, the reconstruction images from all three phantoms are largely encouraging.

V. Summary and outloook

We have demonstrated that long-object imaging using a reverse helical trajectory in the interventional room is feasible using a C-arm system with large motion flexibility such as the Artis zeego system. To process the real data, the calibrated trajectory was first registered to the (x, y, z)-coordinate system, and then an analytical trajectory was found to fit the registered trajectory and its projections were obtained through a rebinning process. Reconstruction results of the torso, CATPHAN and Siemens CB phantoms from the Fusion-RFDK method are encouraging. Note that the modified Artis zeego system is capable of producing a reverse helix consisting of more than five turns, and thus a longer volume is possible.

As mentioned in III-A, the relative angular difference between the fitted and registered trajectories was considerable, and this could yield innegligible resolution loss in the data rebinning step. An alternative approach would be to modify Fusion-RFDK to allow direct usage of the preprocessed registered data for reconstruction. A comparison between this method and the one in this work is the topic of future investigations.

References

[1] S. Cho, D. Xia, C. A. Pellizzari, and X. Pan, "A BPF-FBP tandem algorithm for image reconstruction in reverse helical cone-beam CT," *Med. Phys.*, vol. 37, no. 1, pp. 32–39, Jan 2010.

[2] N. Strobel, B. Heigl, T. Brunner, O. Schuetz, M. Mitschke, K. Wiesent, and T. Mertelmeier, "Improving 3d image quality of x-ray c-arm imaging systems by using properly designed pose determination systems for calibrating the projection geometry," in *Proceedings of SPIE*, vol. 5030, 2003, pp. 943–54.

[3] Z. Yu, F. Noo, F. Dennerlein, G. Lauritsch, and J. Hornegger, "FDK-type reconstruction algorithms for the reverse helical trajectory," in *Proc. IEEE Nuc. Sci. Symp.*, 2011, pp. 3980–3985.

[4] http://www.sawbones.com/products/ortho/category.aspx?9.

[5] http://www.phantomlab.com/products/catphan.php.

[6] http://www.qrm.de/content/products/imagequality/conebeam.htm.

[7] C. Schwemmer, "High-density object removal from x-ray projection images," Master's thesis, Friedrich-Alexander University Erlangen-Nuremberg, 2010.

[8] M. Zellerhoff, B. Scholz, E. Rührnschopf, and T. Brunner, "Low contrast 3D reconstruction from C-arm data," in *Proceedings of SPIE*, vol. 5745, 2005, pp. 646–55.

[9] N. Strobel, O. Meissner, J. Boese, T. Brunner, B. Heigl, M. Hoheisel, G. Lauritsch, M. Nagel, M. Pfister, E. Rührnschopf, *et al.*, "3D imaging with flat-detector C-arm systems," *Multislice CT*, pp. 33–51, 2009.

[10] S. Hoppe, F. Noo, F. Dennerlein, G. Lauritsch, and J. Hornegger, "Geometric calibration of the circle-plus-arc trajectory," *Phys. Med. Biol.*, vol. 52, pp. 6943–60, 2007.